〈Regular Article〉

Verification by Actual Measurement of Theoretical Relationship between Standard Deviation and Wiener Spectrum in Noise Analysis for Digital Radiographic Systems: Verification in One- and Two-Dimensional Wiener Spectrum

Takashi AMANO [1)], Takanori MASUDA [1)], Keiko ARAO [1)]
Shinichi ARAO [1)], Yasuhiko OKURA [2)]

1) Department of Radiological Technology, Faculty of Health Science and Technology, Kawasaki University of Medical Welfare
2) Department of Clinical Radiology, Faculty of Health Science, Hiroshima International University

ABSTRACT **Objective**: This study evaluates image noise using two theoretical equations:: standard deviation (σ) as a spatial domain analysis method and Wiener spectrum (WS) as a spatial frequency domain analysis method. The distinction between the two theoretical equations is that σ^2 corresponds to the area of the one-dimensional (ID) WS and the volume of the two-dimensional (2D) WS. The aim was to investigate these equations using actual X-ray images.

Methods: The X-ray imaging system employed was an AeroDR2 1417HQ (Konica Minolta Japan, Tokyo, Japan), featuring an indirect conversion-type flat panel detector. The 1D WS was obtained using the virtual slit method, while the 2D WS was obtained through the 2D Fourier transform method.

Results: The relative error between σ^2 measured by the virtual slit size and the area of the 1D WS was less than 0.40%. The relative error between σ^2 measured by pixel size and the volume of the 2D WS was close to 0.00%.

Conclusion: The accuracy of both theoretical equations was confirmed with a degree of agreement exceeding 99.5%. These minimal relative errors validated the accuracy of the theoretical equations. Given the requirement for analytical values in 2D images, we propose adopting the equation where σ^2 equals the volume of the 2D WS rather than the equation where σ^2 equals the area of the 1D WS. doi：10.11482/KMJ-E202450097 *(Accepted on November 22, 2024)*

Key words：Noise, Standard deviation, Wiener spectrum, Normalized noise power spectrum, One-dimensional, Two-dimensional

Corresponding author
Takashi Amano
Department of Radiological Technology, Faculty of Health Science and Technology, Kawasaki University of Medical Welfare, 288 Matsushima, Kurashiki, 701-0193, Japan

Phone : 81 86 462 1111
Fax : 81 86 462 1109
E-mail: amano@jc.kawasaki-m.ac.jp

INTRODUCTION

Several methods exist for evaluating image noise, including standard deviation (σ) in the spatial domain, and Wiener spectrum (WS) in the spatial frequency domain. σ is used as the noise value for image quality evaluation in the spatial domain, such as in contrast-to-noise ratio and signal difference-to-noise ratio. WS is used for image quality assessment in the spatial frequency domain and for evaluating the detection efficiency of X-ray imaging systems, such as noise equivalent quanta and detective quantum efficiency. Clarifying the interrelationship between σ and WS is essential for correlating noise and image quality assessments in both the spatial and spatial frequency domains. Additionally, it is possible to convert WS measurement results into σ values for practical use.

Currently, two notations are employed as theoretical formulas to express the interrelationship between σ and WS. One is equation (1), which assumes that the square of σ (variance) is equal to the area of a 1D WS:

$$\sigma^2 = \int_{-\infty}^{\infty} WS(u)\,du \tag{1}$$

The other is equation (2), which assumes that the variance is equal to the volume of a 2D WS:

$$\sigma^2 = \iint_{-\infty}^{\infty} WS(u,v)\,dudv \tag{2}$$

The theoretical correlation equations (1) and (2) have been extensively detailed in academic reports and books in Japan for many years[1-4]. However, there have been no reports of actual measurements validating its accuracy. Recently, Nishiki *et al.* conducted a verification using simulated images[5]. Nonetheless, since various practical considerations must be performed into account when employing actual X-ray images, the system's practical applicability has not been confirmed with actual measured images. Verification using real X-ray images may involve more measurement errors. Therefore, it is necessary to analyze actual X-ray images using a general methodology and verify the validity of the equation based on the results.

In this study, we verify the two theoretical correlation equations using actual X-ray images. Furthermore, we discuss the domestic notations of equations (1) and (2).

MATERIALS AND METHODS

X-ray Imaging System

The X-ray imaging system utilized was the AeroDR2 1417HQ (Konica Minolta Japan, Tokyo, Japan), an indirect conversion-type flat panel detector (FPD) with a cesium iodide (CsI) X-ray conversion unit. The pixel size was 0.175 mm, and the image area measured 348.95×425.25 mm (1995×2430 pixels). A CS-7 workstation from the same manufacturer was used. Image data were saved in RAW format with a dynamic range width (G value) of 4.00 and a fixed system sensitivity (S value). The X-ray generator used was a BLR-500A X-ray tube (Canon Medical Systems Japan, Tokyo, Japan) and a DOCST-03SS console panel from the same manufacturer.

Creating a Noise Image

The radiation quality during the capture of noisy images was RQA5 as per Japanese Industrial Standards (JIS) T 61267:2014[6, 7]. RQA5 represents the radiation quality with a tube voltage set at 70 kV and an additional aluminum filter added to an aluminum plate, resulting in a half-value layer thickness of 6.8 mm. The geometric arrangement for measuring the half-value layer was in accordance with JIS T 61267:2014. The dosimeter used for these measurements was an EMF521 (EMF Japan, Hyogo), and the ion chamber employed was a DC300 (IBA, Schwarzenbruck, Germany). A Model 115A (Kasei Optonix, Kanagawa, Japan) was used for measuring the half-value layer. According to

JIS T 61267:2014, an additional aluminum filter for adjusting radiation quality requires a purity of 99.9% or higher. However, for convenience, an aluminum plate with 99.5% purity (A1050; UACJ, Nagoya) was utilized. The thickness of the additional filter was 21 mm, resulting in radiation quality equivalent to that of RQA5.

Fig. 1 displays the geometric layout diagram used for acquiring noisy images. Because it was not feasible to arbitrarily set the system sensitivity (S value) relative to the distance between the focus and FPD, this distance was fixed at 3 m to ensure the consistent image creation conditions. Additionally, considering the maximum pixel value of the FPD used in this study was 4095, the exposure dose was determined based on specific exposure conditions (70 kV, 50 mA, and 0.125 s), sec), resulting in a pixel value reduced to approximately 2000. The relative dose intervals of 1/8, 1/4, 1/2, standard, and 2, 4, and 8 times the standard dose, with 10 images captured at each relative dose.

Analysis of Noisy Images

A cropped image with a matrix size of 256×256 pixels was generated at the center of the X-ray beam in the noisy image. The average pixel value of the cropped image was then measured to create a digital characteristic curve. The gradient (G) of this curve was determined and used to convert the pixel value into relative X-ray doses.

Next, a quadratic surface approximation function was applied to the cropped image to generate a trend image. Subsequently, the trend image was subtracted from the cropped image to produce a detrended image.

Using the detrended images, we conducted two verification measurements: first, 1D WS and σ were measured using the virtual slit method, and second, 2D WS and σ were measured using the 2D Fourier transform method.

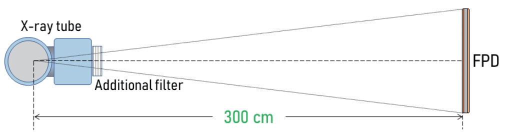

Fig. 1. Geometrical arrangement diagram for noise images.

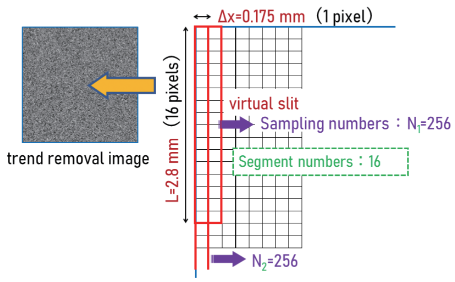

Fig. 2. Diagram of sampling in the virtual slit method.

Measurement of 1D WS and σ using the Virtual Slit Method

The detrended images were sampled using the virtual slit method, as illustrated in Fig. 2. In this method, the virtual slit was configured with an aspect ratio of 16 pixels vertically and 1 pixel horizontally. Sampling involved 256 samples per segment, with a total of 16 segments.

Fig. 3 displays profile data (average pixel value data within the virtual slit) from one measured segment. The virtual slit method performs a 1D Fourier transform on this profile data to obtain a 1D spectrum, $F(u)$. It then computes the u-axis cross-section of the 2D WS, denoted as $WS_{\Delta P}(u, 0)$, utilizing equation (3)[1−4].

$$WS_{\Delta P}(u,0) = L \cdot \frac{\Delta x}{N} \left| F(u) \right|^2 \tag{3}$$

Here, $WS_{\Delta P}(u, 0)$ represents the u-axis cross-section of the 2D WS derived from the noise fluctuation in pixel values, where Δx is the sampling interval (0.175 mm), N is the number of samples (256), and L is the height of the virtual slit (2.8 mm). It is important to note that the virtual slit method incorporates L as a slit correction in equation (3), effectively transforming the 1D WS $WS_{\Delta P}(u)$ into

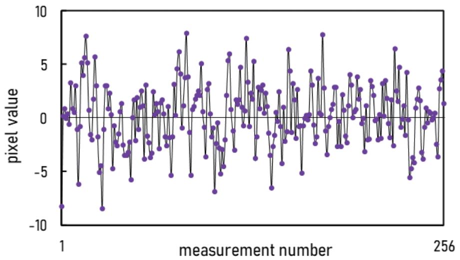

Fig. 3. Profile data for one segment.

2D WS $WS_{\Delta p}(u, 0)$. As a result, 1D WS $WS_{\Delta P}(u)$ is computed through the inverse transformation of equation (4).

$$WS_{\Delta P}(u) = \frac{WS_{\Delta p}(u, 0)}{L} \quad (4)$$

Furthermore, the noise fluctuation of the pixel values, $WS_{\Delta P}(u)$, was transformed into the noise fluctuation of the X-ray dose normalized by the average X-ray dose $\bar{E}$: $WS_{\Delta E/\bar{E}}(u)$, using equation (5)[8-13].

$$WS_{\Delta E/\bar{E}}(u) = \frac{1}{(\log_{10} e)^2 \cdot G^2} \cdot WS_{\Delta P}(u) \quad (5)$$

Here, G represents the slope of the digital characteristic curve. The results from the 16 measured segments were averaged to obtain the results for each image. Subsequently, the 1D WS for 10 images was averaged to obtain the final result.

Next, the pixel value σ : $\sigma_{\Delta P}$ was computed using equation (6), based on the measurement data (256 pieces) of noise fluctuation for one segment in Fig. 3.

$$\sigma_{\Delta p} = \sqrt{\frac{\sum (P - \overline{P})^2}{(N-1)}} \quad (6)$$

Here, P represents the pixel value of the noise fluctuation; $\overline{P}$ denotes the average pixel value of the noise fluctuation; and N denotes the number of data points (256). Then, the X-ray dose-normalized standard deviation σ : $\sigma_{\Delta E/\bar{E}}$ was computed using equation (7).

$$\sigma_{\Delta E/\bar{E}} = \frac{1}{\log_{10} e \cdot G} \cdot \sigma_{\Delta P} \quad (7)$$

The results from the 16 measured segments were averaged to obtain the results for a single image. Subsequently, $\sigma_{\Delta E/\bar{E}}$ for 10 images was averaged to yield the final result.

Measurement of 2D WS and σ using the 2D Fourier Transform Method

A 2D Fourier transform was applied to the pixel value data (256 × 256) from the detrended image to generate the 2D spectrum $F(u, v)$, which was subsequently transformed into 2D WS $WS_{\Delta P}(u, v)$ using equation (8)[14].

$$WS_{\Delta P}(u, v) = \frac{\Delta x \cdot \Delta y}{N_x \cdot N_y} \cdot |F(u, v)|^2 \quad (8)$$

Here, Δx, Δy represent the sampling intervals (0.175 mm), while N_x, N_y denote the matrix size (256). Subsequently, the noise fluctuation of the pixel values, $WS_{\Delta P}(u, v)$, was transformed into the noise fluctuation of the X-ray dose normalized by the average X-ray dose $\bar{E}$ using equation (9): $WS_{\Delta E/\bar{E}}(u, v)$.

$$WS_{\Delta E/\bar{E}}(u, v) = \frac{1}{(\log_{10} e)^2 \cdot G^2} \cdot WS_{\Delta P}(u, v) \quad (9)$$

The 2D WS for the 10 images was averaged to yield the final outcome.

Subsequently, the pixel value σ : $\sigma_{\Delta P}$ was computed using equation (6) based on the pixel value data (256 × 256) of the detrended image. This value was then converted to the X-ray dose σ : $\sigma_{\Delta E/\bar{E}}$, normalized by the average X-ray dose $\bar{E}$, using equation (7). Finally, the $\sigma_{\Delta E/\bar{E}}$ for the 10 images was averaged to obtain the ultimate result.

To calculate the integral of the Wiener spectrum

The integral over the area of the 1D WS, denoted as $WS_{\Delta E/\bar{E}}(u)$ in equation (1), was computed using equation (10).

$$Area = \int_{-nf}^{nf} WS_{\Delta E/\bar{E}}(u)\,du \tag{10}$$

Similarly, the integration over the volume of the 2D WS, represented as $WS_{\Delta E/\bar{E}}(u, v)$ in equation (2), was performed using equation (11).

$$Volume = \iint_{-nf}^{nf} WS_{\Delta E/\bar{E}}(u, v)\,du\,dv \tag{11}$$

Here, nf represents the Nyquist frequency (cycles/mm) and nf = 2.857. Given that the actual data are discrete, the integral computation utilizes the rectangular rule for both 1D and 2D WS.

Calculating the relative error

To verify the correctness of equations (1) and (2), we calculated the relative error between the square of σ measured using the virtual slit size: $\sigma_{\Delta E/\bar{E}}$ and the area integral value of 1D WS $WS_{\Delta E/\bar{E}}(u)$, and the relative error between the square of σ measured using the pixel size: $\sigma_{\Delta E/\bar{E}}$ and the volume integral value of 2D WS $WS_{\Delta E/\bar{E}}(u, v)$, confirming the degree of agreement. The relative error was calculated to three significant digits because the minimum pixel value of the noisy image was three digits.

RESULTS

Fig. 4 depicts the measurement outcomes of the digital characteristic curves. The FPD employed in this investigation operates on a logarithmic system, and it was validated that the logarithmic values of the relative X-ray dose and the pixel value exhibited an accurate linear correlation. The gradient (G) of the digital characteristic curve was determined to be 1033.23.

Fig. 5 display the 1D WS $WS_{\Delta E/\bar{E}}(u)$ for each relative dose obtained using the virtual slit method. The definition of the 1D WS is given by equation (12) based on the relationship between equations (3) and (4), where the unit is Δx in mm and it has a length dimension.

$$WS_{\Delta P}(u) = \frac{\Delta x}{N}|F(u)|^2 \tag{12}$$

Based on the results shown in Fig. 5, the area integral value was calculated using equation (10). Fig. 6 shows the 2D WS $WS_{\Delta E/\bar{E}}(u, v)$ for each relative dose obtained using the 2D Fourier transform method. The unit of the 2D WS obtained from equation (8) is mm^2 and it has the dimension of area. Based on the results shown in Fig. 6, the volume integral was calculated using equation (11).

Table 1 presents the relative error results for each relative dose. The relative error between the square of σ measured using the virtual slit size $\sigma_{\Delta E/\bar{E}}$ and

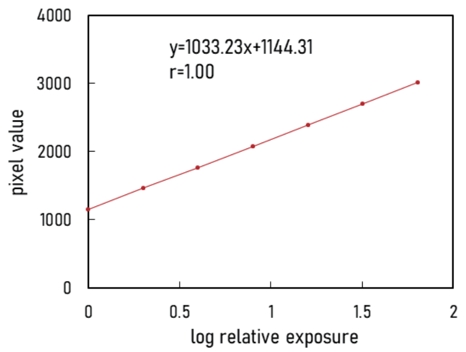

Fig. 4. Digital characteristic curve of the flat panel detector.

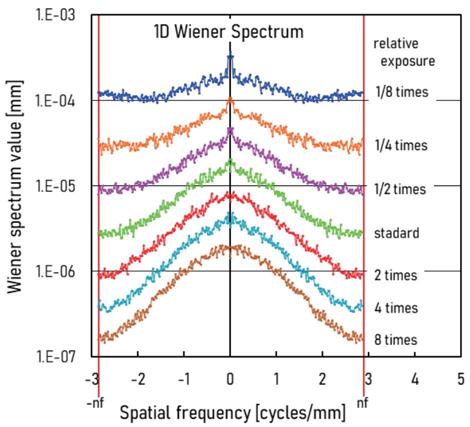

Fig. 5. 1D WS measured by the virtual slit method.

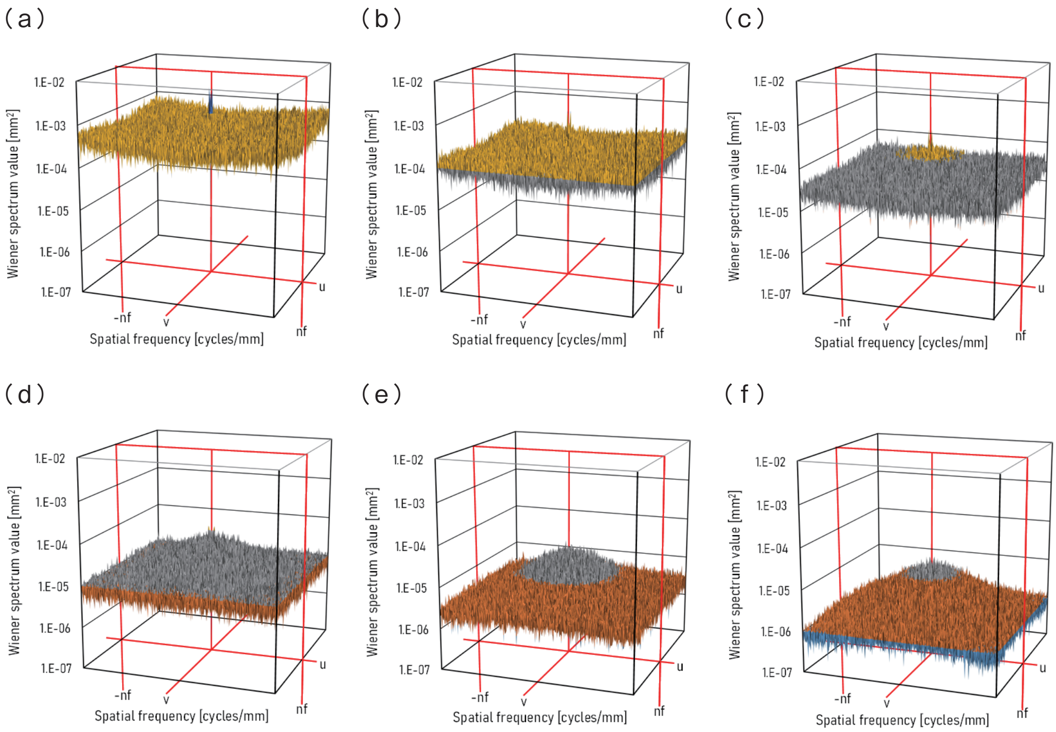

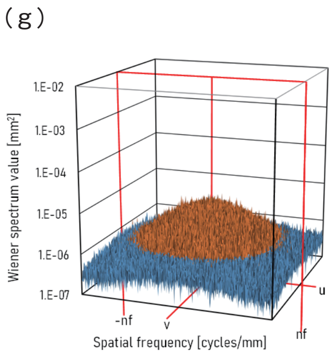

Fig. 6. 2D WS measured by the 2D Fourier transform method.
(a) 1/8 times of standard dose
(b) 1/4 times of standard dose
(c) 1/2 times of standard dose
(d) standard dose
(e) 2 times of standard dose
(f) 4 times of standard dose
(g) 8 times of standard dose

the area integral value of the 1D WS $WS_{\Delta E/\bar{E}}(u)$ was less than 0.40%, although it varied depending on the shooting conditions. In addition, the relative error between the square of σ measured using the pixel size $\sigma_{\Delta E/\bar{E}}$ and the volume integral value of 2D WS $WS_{\Delta E/\bar{E}}(u, v)$ was close to 0.00%.

DISCUSSION

When calculating the relative error with three significant digits, the maximum potential rounding error was 0.5%. Therefore, if the calculated relative error falls at or below 0.5%, it may not reliably indicate differences. However, given that the computed relative error remained at 0.5% or less, it can be asserted that the degree of agreement between these equations surpasses 99.5%. With relative errors associated with equations (1) and (2) below 0.40% and approaching 0.00%, respectively, the degree of agreement between these equations surpassed 99.5%. Therefore, we confirm the

Table 1 Relative error between the square of standard deviation and area of 1D WS, and relative error between square of standard deviation and the volume in the 2D WS.

exposure dose	1D WS σ^2	$\int_{-nf}^{nf} WS(u)\,du$	relative error	2D WS σ^2	$\iint_{-nf}^{nf} WS(u,v)\,dudv$	relative error
1/8 times	7.69E-04	7.70E-04	0.13%	1.21E-02	1.21E-02	0.00%
1/4 times	2.50E-04	2.51E-04	0.40%	3.49E-03	3.49E-03	0.00%
1/2 times	9.83E-05	9.83E-05	0.00%	1.16E-03	1.16E-03	0.00%
Standard	4.16E-05	4.16E-05	0.00%	4.26E-04	4.26E-04	0.00%
2 times	1.87E-05	1.87E-05	0.00%	1.75E-04	1.75E-04	0.00%
4 times	9.07E-06	9.08E-06	0.11%	7.99E-05	7.99E-05	0.00%
8 times	4.52E-06	4.53E-06	0.22%	3.90E-05	3.90E-05	0.00%

complete accuracy of both equations. Also, the slightly larger relative error observed at 1/4 and 8 times compared to other conditions is not due to increased error under specific dose conditions, however rather attributable to stochastic variation.

During our investigation and comparison of equations (1) and (2) as depicted in the literature, particularly in textbooks, academic papers, and reference works, we observed a scarcity of instances where both equations were presented simultaneously[1]. There appears to be a balanced distribution between descriptions of equation (1)[4, 13, 15–17], which asserts that the square of σ equal the surface integral value of a 1D WS, and descriptions of equation (2)[2, 3, 18, 19], which posits that the square of σ corresponds to the volume integral value of a 2D WS. Traditionally, X-ray images are 2D, which naturally leads to the focus on 2D analysis results in WS measurements. When using the virtual slit method, the 1D WS is initially measured and then it is converted into either the u-axis cross-section $WS(u, 0)$ or v-axis cross-section $WS(0, v)$. On the other hand, the 2D Fourier transform method directly measures the 2D WS $WS(u, v)$ as illustrated in Fig. 6. However, for display purposes, it often utilizes the u-axis or the v-axis cross-sections of the 2D WS. Thus, when a 2D image is the measurement target, the 2D WS is calculated instead of the 1D WS. Similarly, the modulation transfer function (MTF) is calculated by either performing a 2D Fourier transform on the point spread function to measure the absolute value and normalized 2D MTF: $MTF(u, v)$, or by performing a 1D Fourier transform on the line spread function to measure the absolute value and normalized 2D MTF's u-axis cross-section $MTF(u, 0)$ and v-axis cross-section $MTF(0, v)$.

In practical applications, WS and MTF modulations rarely yield analytical results in a single dimension. Therefore, we advocate prioritizing equation (2), which establishes the interrelationship in 2D, over equation (1), which defines it in 1D.

In an additional experiment, we verified whether σ, 1D WS, and 2D WS, measured at pixel size, satisfy equation (13).

$$\sigma_{\Delta E/\bar{E}}{}^2 = \int_{-nf}^{nf} WS_{\Delta E/\bar{E}}(u)\,du = \iint_{-nf}^{nf} WS_{\Delta E/\bar{E}}(u, v)\,dudv \tag{13}$$

Verification was conducted using only a noisy image of the standard dose. The volume integral value on the left side of $\sigma_{\Delta E/\bar{E}}{}^2$ and the right side of 2D WS $WS_{\Delta E/\bar{E}}(u, v)$ have already been measured (Table 1, 2D WS, Standard), leaving only the area integral value of the middle term 1D WS $WS_{\Delta E/\bar{E}}(u)$ to be measured. The measurement utilized 256 segments (one image), which required numerous calculations. Concurrently, for equation (13) to hold true for the right-hand and middle terms, the relationship between 1D WS $WS_{\Delta E/\bar{E}}(u)$ and 2D WS $WS_{\Delta E/\bar{E}}(u, v)$ must satisfy equation (14). Thus, we verify equation (14).

$$WS_{\Delta E/\bar{E}}(u) = \int_{-nf}^{nf} WS_{\Delta E/\bar{E}}(u, v)\, dv \qquad (14)$$

Equation (14) denotes a relational equation indicating that the 1D WS $WS_{\Delta E/\bar{E}}(u)$, obtained by projecting (line integral) the 2D WS $WS_{\Delta E/\bar{E}}(u, v)$ on the right-hand side onto the v-axis direction (as illustrated in Fig. 6(d)), equals the 1D WS $WS_{\Delta E/\bar{E}}(u)$ measured by setting the height of the virtual slit to 1 pixel on the left-hand side.

Following the verification of equation (13), the area integral value of the middle term $WS_{\Delta E/\bar{E}}(u)$ was found to be 4.29×10^{-4}, closely matching the value of 4.26×10^{-4} on both the left and right sides (relative error: 0.70%), confirming the validity of equation (13). Additionally, when comparing and graphing the measurement results of the left and right sides of equation (14) (Fig. 7), they were found consistent with each other and with the verification results using CT simulation noise images by Narita *et al.*[20]. This demonstrates that the projection (line integral) of the 2D WS $WS(u, v)$ in the v-axis direction is equivalent to the 1D WS $WS(u)$. However, unlike equation (13), there is no

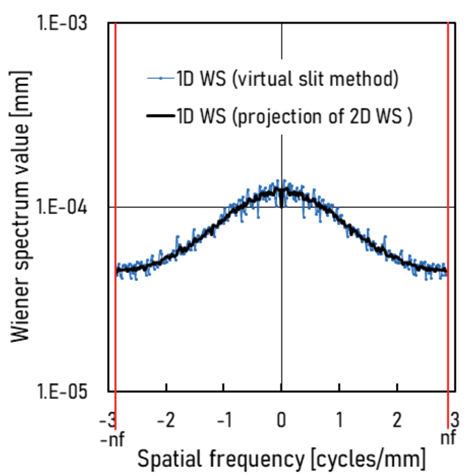

Fig. 7. Comparison of the 1D WS obtained by the virtual slit method (slit height and width: 1 pixel) and the 1D WS obtained by projection of the 2D WS.

correlation between $\sigma_{\Delta E/\bar{E}}^{2}$ in equation (15) and the area integral value of the u-axis cross-section of 2D WS $WS_{\Delta E/\bar{E}}(u, 0)$.

$$\sigma_{\Delta E/\bar{E}}^{2} \neq \int_{-nf}^{nf} WS_{\Delta E/\bar{E}}(u, 0)\, du \qquad (15)$$

Caution is necessary when using WS measurement results converted to σ or when comparing WS and σ results. Additionally, the u-axis cross-section of 2D WS $WS_{\Delta E/\bar{E}}(u, 0)$ and the u-axis cross-section of 2D MTF $MTF(u, 0)$ are occasionally denoted as $WS_{\Delta E/\bar{E}}(u)$, representing 1D WS, and $MTF(u)$, representing 1D MTF. However, these data are essentially a 1D array and the values are derived from 2D analyses; therefore, meticulous care is required in notation and differentiation between them.

With the validation of equations (1) and (2), it has become possible to integrate visual characteristics into the spatial domain noise analysis value, σ, which was previously challenging. By scaling the spatial frequency domain noise analysis value, WS, with the visual response function and converting it to σ, it is anticipated that a σ value that incorporates visual characteristics can be computed. Moreover, with the advent of CT and MRI technologies, opportunities to use three-dimensional images have increased, leading to a rise in the number of research reports on 3D WS recently[21-24]. In the future, we expect to see the development and validation of multidimensional analyses, including extending equation (2) to three dimensions[23] and exploring 3D MTF analysis[24].

LIMITATIONS

Our study has several limitations. First, it is necessary to conduct experiments using beam qualities other than RQA5 to determine whether the relative error is dependent on beam quality. Second, the experiment should be repeated with varying numbers of measurements to assess whether the relative error is influenced by the number of measurements. Lastly, further investigation is required to identify the cause of the larger relative error in equation (1) compared to equation (2).

CONCLUSION

Verification conducted using actual X-ray images revealed that the relative error of the correlation equation, assuming the square of σ equals the area of 1D WS, was less than 0.40% at three significant digits. Similarly, the relative error of the correlation equation, equating the square of σ to the volume of 2D WS, was close to 0.00%. This confirms the accuracy of both correlation equations, with the degree of agreement exceeding 99.5%. We also validated the relationship between 1D WS and 2D WS, affirming the reliability of the theoretical formulation. Moreover, we suggest prioritizing the correlation equation where the square of σ equals the volume of 2D WS.

FUNDING

This research received no grant or other funding

CONFLICT OF INTEREST STATEMENT

The first author and all co-authors have no conflicts of interest to declare.

REFERENCES

1) Kodera Y, Oohisa T, Tanaka I, Okada H, Kondo T, Fujimura Y, Masuya R, Yamashita K: Methods of measuring granularity in radiographic systems(I). Japanese Journal of Radiological Technology. 1987; 43 (12). 1743-1768. doi: 10.6009/jjrt.kj00001364005.

2) Tanaka K: Wiener spectrum. Basic Image Engineering of Radiography (Uchida M, Kodera Y, Fujita H). Tokyo, Ohmsha. 2003. pp.132-143.

3) Yoshida A: Physical Image Quality of Radiographic Systems - Basic Concept and Theory. Humanity and Science: Journal of the Faculty of Health and Welfare, Prefectural University of Hiroshima. 2014; 14 (19): 1-22.

4) Ishida T, Matsumoto M, Kano A, Shimosegawa M: Easy to Understand Medical Image Engineering. Second ed. Tokyo, Ohmsha. 2015. pp.91-109.

5) Nishiki M, Doi K: Dimensional conversion of Wiener spectrum learned from "Image Science". Japanese Journal of Radiological Technology, Image Communication. 2021; 44 (2). 35-43.

6) JIS T 61267: Medical diagnostic X-ray equipment - Radiation conditions for use in the determination of characteristics. 2014.

7) IEC 61267: Medical Diagnostic X-ray Equipment - Radiation Conditions for use in the Determination of Characteristics. 2005.

8) Yamazaki T: Practical Measurements of the Digital Winner Spectrum. Tokyo, Innervision. 2003; 18 (12). pp.40-46.

9) Asahara M: Noise Power Spectrum. Japanese Journal of Radiological Technology. 2009; 65 (12). 1671-1679.

10) Asahara M: Characteristics of Noise. Handbook of Medical Imaging (Ishida T, Katsuragawa S, Fujita H). Tokyo, Ohmsha. 2010. pp.515-527.

11) Kunitomo H: Noise Characteristics and NNPS Analysis in Digital X-ray Images. Japanese Journal of Radiological Technology, Image Communication. 2013; 36 (1). 78-86.

12) Kunitomo H: Noise Characteristics. Medical Imaging and Information Engineering. Second ed. (Teramoto A, Fujita H). Tokyo, Ishiyaku Publishers. 2010. pp.57-64.

13) Katsuragawa S: Medical Imaging and Information Sciences. Forth ed. Tokyo, Nanzando. 2020. pp.99-115.

14) Kunitomo H: Noise Characteristics. Image Quality Measurement of Digital Radiography. (Ichikawa K, Ishida T). Tokyo, Ohmsya. 2010. pp.172-210.

15) Okumura E: Noise Characteristics. Practice! Medical Imaging and Information Sciences - From Basics to Experiments and Exercises. (Fukushi M, Hashimoto T). Tokyo, Medical View. 2020. pp.195-202.

16) Morishita J: Granularity (Noise Characteristics). Radiological technologist, National Examination Preparation for All subjects (Nishitani M, Endo K, Akazawa H). Fourteen ed. Tokyo, Kinpodo. 2022. pp.321-322.

17) Kondo K: Image Engineering. National Examination of Radiological technologist, Passed! My Text. Fiscal Year 2024 Ed. (Murakami K). Fourteen ed. Tokyo, Ohmsya. 2023. pp.791-813.

18）Fujita H, Yamashita K: Analysis and Evaluation of Images. Clinico-Radiologicl Technology (Kozuka T, Inamura K, Doi T, Sumida I). Fourteen ed. Tokyo, Nankodo. 2019. pp.30-48.

19）Shimosegawa M, Hoshino S, Sekine N, Nyui Y, Abe S, Omatsu M: Medical Imaging and Information Sciences. Tokyo, Iryokagakusya. 2010. p.120.

20）Narita A, Ohkubo M, Fukuya T, Noto Y: Central Slice Theorem-based Relationship between 1D-NPS Obtained by the Slit Method and 2D-NPS for CT Images. Japanese Journal of Radiological Technology. 2021; 77 (8). 828-832. doi: 10.6009/jjrt.2021_JSRT_77.8.828.

21）Narita A, Ohkubo M, Ohsugi Y, Sakai K, Fukuya T, Noto Y: A Study of Longitudinal NPS Measurement in CT Images Based on the Central Cross-section Theorem. Japanese Journal of Radiological Technology. 2021; 77 (8). 828-832. doi: 10.6009/jjrt.2022-1267.

22）Narita A, Ohkubo M, Fukuya T, Sakai K, Noto Y: A Study of 3D-NPS Analysis in CT Images Based on the Central Cross-section Theorem. Japanese Journal of Radiological Technology. 2022; 78 (4). 342-347. doi: 10.6009/jjrt.2022-1217.

23）Tward DJ, Siewerdsen JH: Cascaded Systems Analysis of the 3D Noise Transfer Characteristic of Flat-Panel Cone-Beam CT, Med phys, 2008; 35 (12), 5510-5529. doi: 10.1118/1.3002414.

24）Chen B, Christianson O, Wilson JM, Samei E: Assessment of Volumetric Noise and Resolution Performance for Linear and Nonlinear CT Reconstruction Methods, Med phys, 2014; 41 (7), 071909. doi: 10.1118/1.4881519.